Serra Alfaro, José Manuel;Escolástico Rozalén, Sonia;Solis Díaz, C.;Kjølseth, C. (2017). Catalytic Layer Optimization for Hydrogen Permeation Membranes Based on La5.5WO11.25-d;/La0.87Sr0.13CrO3-d; Composites. ACS Applied Materials & Interfaces. 9(41):35749-35756. https://doi.org/10.1021/acsami.7b08995

Catalytic layer optimization for hydrogen permeation membranes based on $La_{5.5}WO_{11.25-\delta}/La_{0.87}Sr_{0.13}CrO_{3-\delta}$ composites

Sonia Escolástico[a], Cecilia Solis[a], Christian Kjølseth[b] and Jose Manuel Serra[a,*]

[a] *Instituto de Tecnología Química (Universitat Politècnica de València - Consejo Superior de Investigaciones Científicas) Avenida de los Naranjos s/n.46022 Valencia, Spain.*

[b] *Coorstek Membrane Sciences, Forskningsparken, Gaustadalleèn 21, NO-0349 Oslo, Norway*

** corresponding author: jmserra@itq.upv.es*

Keywords: hydrogen permeation, proton conductor, catalytic layer, sputtering, metallic layers

Abstract

(LWO/LSC) composite is one of the most promising mixed ionic-electronic conducting materials for hydrogen separation at high temperature. However, these materials present limited catalytic surface activity towards H_2 activation and water splitting, which determines the overall H_2 separation rate. For the implementation of these materials as catalytic membrane reactors, effective catalytic layers compatible and stable under the reaction conditions have to be developed. This contribution presents the development of catalytic layers based on sputtered metals (Cu and Pd), the electrochemical characterization by impendace spectrocopy and the study of the H_2 flow obtained by coating them on 60/40-LWO/LSC membranes. Stability of the catalytic layers is also evaluated under H_2 permeation conditions and CH_4-containing atmospheres.

1. Introduction

Mixed protonic-electronic conductors have been widely studied in the last years for their application as hydrogen separation membranes at high temperature (500 -1000 ºC). Membranes made with this kind of materials present several advantages: (a) membranes are totally dense and present infinite H_2 permselectivity, (b) protonic transport occurs without external current application, (c) their operational window matches the requirements of several appealing chemical reactions; and (d) their surface has negligible activity towards hydrocarbon coking under non-oxidative conditions. Catalytic membranes reactors based on ceramic mixed protonic-electronic conductors enables to combine in a single step H_2 separation and chemical reaction, which gives rise to energy savings and strong improvements in the per-pass product yield for

equilibrium-limited reactions[1-3]. Different reactions can be performed in this kind of membrane reactors: dehydrogenation reactions as methane coupling[4], methane dehydroaromatization (MDA)[5-9] or steam reforming (SMR)[10-12].

Composites made of $La_{5.5}WO_{11.25-\delta}$ (LWO) and $La_{0.87}Sr_{0.13}CrO_{3-\delta}$ (LSC) have allowed reaching[13-14] one of the highest H_2 flows reported nowadays for ceramic-ceramic composites[15-19]. This high H_2 flow together with their good stability under CO_2 containing atmospheres make these materials as promising candidates for their application as hydrogen separation membranes.[13, 20] Nevertheless, LWO/LSC materials present poor catalytic activity and the development of compatible catalytic layers is mandatory for their industrial application[21]. The required properties of the catalytic layers are: high catalytic activity towards hydrogen evolution and water splitting, high electronic conductivity, redox stability and coking tolerance. A variety of metals have been used as fuel electrode materials for solid oxide fuel cell anodes[22-23] or as catalytic layers in gas permeation membranes[24-25] and several precious metals are reported to function as steam reforming catalyst[26] which indicates that metals could be used also as catalytic layers in hydrogen separation membranes[27]. In this context, copper is a good candidate due to: (a) its low coking activity[28-32] and (b) its important catalytic activity, proved in oxygen permeable membranes.[24] Specifically, the incorporation of copper in a barium strontium cobalt based membrane forms an amorphous matrix rich in copper giving rise to a significant increase of the surface reaction constant, i.e., an increase of the catalytic activity. On the other hand, deposition of catalytic layers can be performed by different techniques. Sputter deposition technique is a broadly used method for preparation of variety of thin layers due to the control of the film thickness, thickness uniformity and a good layer adhesion. In addition, sputtering allows reducing the material costs by achieving thin layers.

This work presents the development of different catalytic coatings based on Cu metal sputtered thin films compatible with LWO/LSC materials and the study of their influence on the H_2 permeation of 60/40-LWO/LSC membranes. The electrochemical behavior of the two different metal sputtered layers is studied by impedance spectroscopy using symmetric cells supported on $BaZr_{0.7}Ce_{0.2}Y_{0.1}O_{3-\delta}$ (BZCY72) electrolyte – a pure proton conductor. Finally, the stability of the catalytic layers is also evaluated under H_2 permeation conditions and under CH_4-containing atmospheres.

2. Experimental

60% $La_{5.5}WO_{11.25-\delta}$-40% $La_{0.87}Sr_{0.13}CrO_{3-\delta}$ (hereafter 60/40-LWO/LSC) composite was prepared by mixing the corresponding amounts of LWO (provided by Cerprotech (NO) and calcined at 800 ºC) and LSC (provided by Praxair (US) and calcined at 900 ºC). Both materials were ball-milled together for 24 hours.

Crystalline phases were identified by X-ray diffraction (XRD) performed in a CubiX FAST equipment using $CuK\alpha_{1,2}$ radiation and an X'Celerator detector in Bragg-Brentano geometry in the 2θ range from 20 to 70º. XRD patterns were analyzed using X'PertHighscore Plus software (PANalytical).

Composite membranes used in H_2 permeation measurements consisted of 800 µm-thick gastight discs of 15 mm diameter. Membranes were prepared by uniaxially pressing at 72 MPa of the mixtures before sintering at 1550 °C for 6 h in air. In order to promote the surface reactions, three different coatings were prepared: (a) a porous Pt thick film (used as a reference membrane) named Pt 60/40-LWO/LSC; (b) Cu thin films henceforth Cu 60/40-LWO/LSC; and (c) Cu+Pd thin films hereafter Cu-Pd 60/40-LWO/LSC.

Pt catalytic layer was obtained by screen-printing the Pt ink (Mateck) on both sides of 60/40-LWO/LSC membrane and the final film thickness was 10 µm. Sputtered metals Cu and Cu-Pd thin films were deposited with a radio frequency (13.56 MHz) Pfeiffer Classic 250 deposition system equipped with three magnetron guns. The thin films were obtained by sputtering 1 inch Cu and Pd sputtering targets on a rotating substrate holder, with r.f. power of 25 W. Cu thin films were deposited for 4 h and afterwards Pd was deposited for 1 minute. The base pressure of the chamber before the deposition was 2×10^{-6} mbar or lower. In order to optimize the sputtering parameters, Cu was deposited on quartz substrates. The working pressure was 2.1×10^{-2} mbar by using pure Ar. The distance target - substrate was kept to 5 cm and the substrate temperature was 150 ºC. After the deposition films were annealed at 700 ºC for 4 h under dry 5% H_2 atmosphere. Details of the measured membranes such as thickness and quantity of metal (theoretically calculated) in the catalytic layers are given in Table 1.

Table 1: Nomenclature and description of the measured membranes

Nomenclature	Membrane thickness (μm)	Catalytic layer	Coated metal ($g \cdot cm^{-2}$)
Pt 60/40-LWO/LSC	360	Pt	$1.61 \cdot 10^{-2}$
Cu 60/40-LWO/LSC	360	Cu	$1.21 \cdot 10^{-3}$ (Cu)
Cu-Pd 60/40-LWO/LSC	370	Cu+Pd	$1.21 \cdot 10^{-3}$ (Cu) $8.00 \cdot 10^{-5}$ (Pd)

Permeation measurements were performed on a double chamber quartz reactor following the procedure explained elsewhere[33-36]. Argon was used as sweep gas (150 $mL \cdot min^{-1}$) on the permeate side whereas a mixture of H_2-He (100 $mL \cdot min^{-1}$) was fed to the hydrogen-rich chamber.

Permeation measurements were performed under four hydration degree configurations: (C1) dry atmosphere in both sides of the membrane (feed and permeate side); (C2) feed side humidified (pH_2O=0.025 atm); (C3) both membrane sides humidified (pH_2O=0.025 atm); and (C4) sweep side humidified (pH_2O=0.025 atm). In addition, H_2 permeation was checked by using 30% CH_4, 50% H_2 and 20% He as feed, in order to check the stability and catalytic activity of the sputtered layers under CH_4 containing atmospheres.

The H_2 content in the permeate side was analyzed using micro-GC Varian CP-4900 equipped with Molsieve5A and PoraPlot-Q glass capillary modules. H_2 flows expressed as $mL \cdot min^{-1} \cdot cm^{-2}$ were calculated at standard conditions, i.e. expressed in Normal mL. $\cdot min^{-1} \cdot cm^{-2}$. Each condition was analyzed three times and the data are the average of these analyses with an experimental standard deviation ranging between 10^{-3} and 10^{-4}. GC analyses were performed after 30 minutes of stabilization in the steady state.

Symmetrical cells with metal/BZCY72/metal catalytic activation layers were tested by electrochemical impedance spectroscopy (EIS) in two-point configuration with Pt current collector meshes. Input signal was 0 V DC-20 mV/AC in the $0.03\text{-}1 \cdot 10^6$ Hz frequency range (Solartron 1470E and a 1455A FRA module equipment). EIS measurements were performed in the 650-900 ºC range, under wet atmospheres (2.5

vol.% H_2O) at different pH_2 with a constant flow rate of 100 mL min^{-1}. The contribution of the BZCY72 electrolyte was corrected from impedance spectra. BZCY72 dense electrolytes (around 1 mm-thick) were obtained by uniaxially pressing the ball-milled BZCY72 powder (Cerpotech commercial powder) at 120 MPa and finally firing at 1450 ºC for 5 h.

The microstructure of the catalytic layers and membranes was investigated using field emission scanning electron microscopy (FE-SEM) (Zeiss Ultra 55) after the permeation measurements. The integrity of the samples was also checked by XRD.

3. Results and discussion

Cu and Cu-Pd layers were deposited at 150 ºC by magnetron sputtering on both sides of the 60/40-LWO/LSC membranes. XRD patterns of 60/40-LWO/LSC membranes sintered at 1550 ºC with Cu and Cu-Pd layers deposited on the surface are shown in Figure 1 (*y* axis in *log* scale). Only diffraction peaks corresponding to the fluorite (LWO) and the perovskite (LSC) structure are detected in addition to the peaks associated with Cu from the catalytic layers, indicating the compatibility and stability of the LWO/LSC composite and Cu layers after the annealing in H_2. No traces of Pd can be detected in the XRD patterns. This fact could be due to the very small amount of sputtered Pd, only spread on the surface of the Cu layer (see Table 1). On the other hand, the peak at 43.6º that corresponds to Cu is slightly shifted to the left when Pd is also deposited. This small shift could indicate the formation of Cu/Pd alloy as it has been previously reported for Cu electrodes deposited by ELP (electroless plating) and calcined at 750 ºC.[37] This fact was also checked by EDX. Figure S1 shows an EDX mapping of the Cu-Pd sputtered layer on LWO/LSC membrane. Pd-rich grains can be detected on the top of the coating as it is observed in the mapping. Nevertheless, Cu is also detected in the same area. The detection of the Cu also in these grains can be ascribed to the formation of a Cu/Pd alloy or to the sampling depth that corresponds to 1.2 μm in Pd at 20 kV.[37]

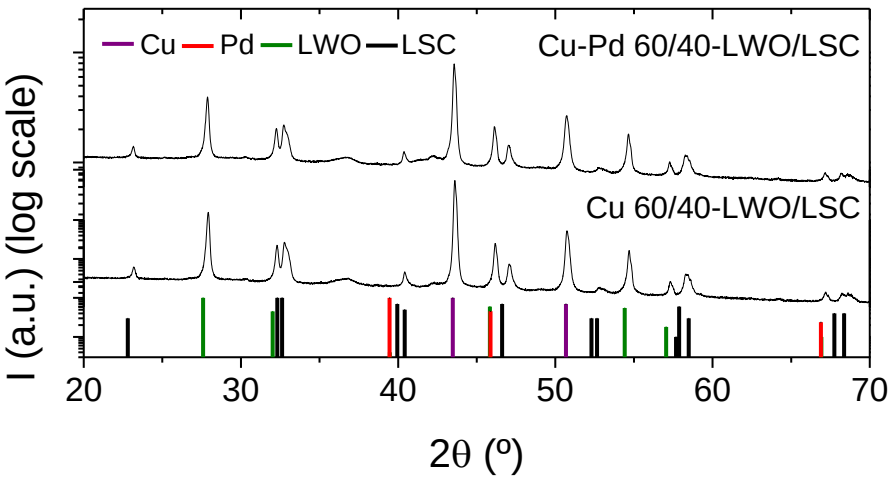

Figure 1: XRD patterns of 60%-LWO/LSC membranes sputtered with Cu and Cu-Pd catalytic coatings.

H_2 permeation flows for the membranes coated with Pt (as reference sample), Cu and Cu-Pd layers were measured under four different hydration conditions (C1, C2, C3 and C4) feeding 50% H_2 in He. Obtained H_2 flows (expressed as $mL \cdot min^{-1} \cdot cm^{-2}$ and $mol \cdot s^{-1} \cdot cm^{-2}$) as a function of the temperature are plotted in Figure 2. The behavior depending on the hydration configuration is very similar for the three membranes under C1, C2 and C3 conditions: in C1 conditions, H_2 flow is very low due to the lack of protonic charge carriers under dry conditions. When H_2 feed side is humidified (C2), H_2 flow increases due to the hydration of the membrane and the consequent incorporation of protons in the structure. When both sides are humidified (C3), the H_2 flow increases reaching values up to 0.22 $mL \cdot min^{-1} \cdot cm^{-2}$. This important rise is ascribed to the higher H_2 flux through the membrane because of the higher hydration in addition to the H_2 formation by water splitting reaction in the sweep side as a result of the oxide-ion transport from the sweep side to the feed side.[33-34, 38] Finally, when only the sweep gas is humidified (C4), different behaviors are observed: Pt and Cu-Pd membranes present lower H_2 flow under C4 than under C3 as it is expected from the higher proton character of the material in this range of temperature. The lower hydration degree of the oxide leads to the reduction of the proton flux through the membrane. However, for Cu coated sample, H_2 flow is higher under C4 above 650 ºC. This effect could be related with the lower catalytic activity of Cu for the H_2 bond breaking, as compared with Pt and Cu-Pd that leads to a higher contribution of the water splitting to the total H_2 flow.

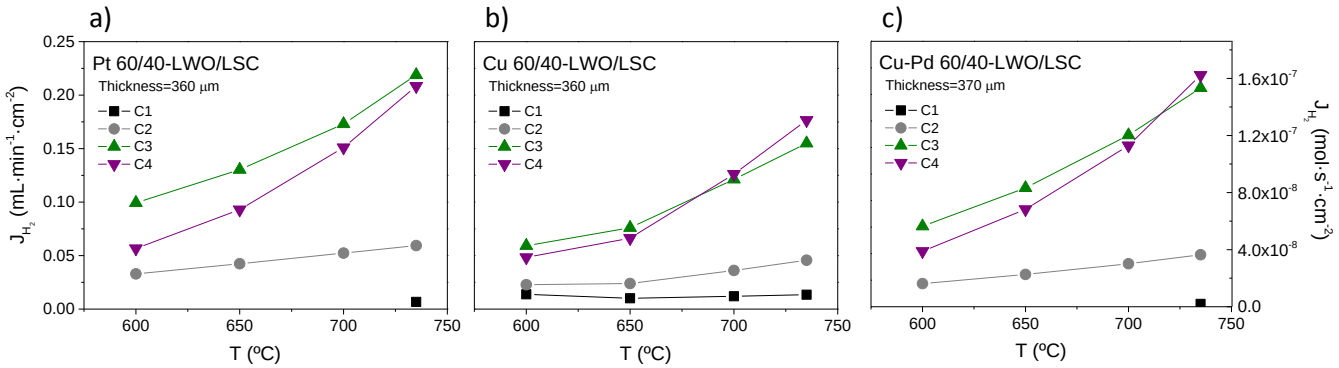

Figure 2: H_2 flow (expressed as $mL \cdot min^{-1} \cdot cm^{-2}$ and $mol \cdot s^{-1} \cdot cm^{-2}$) as function of temperature for 60%-LWO/LSC with different catalytic coatings: (a) screen-printed Pt, (b) Cu and (c) Cu-Pd sputtered metals in four different hydration degree configurations: C1, C2, C3 and C4 feeding 50% H_2. Experimental standard deviation ranges between 10^{-3} and 10^{-4}.

Normalized H_2 flows (expressed as $mL \cdot min^{-1} \cdot cm^{-1}$, in order to disregard the influence of the membrane thickness) for the Pt, Cu and Cu-Pd coated membranes are compared in Figure 3 for C2, C3 and C4 conditions. Cu-Pd coated membrane presents slightly lower H_2 flows than Pt activated membrane in the whole range of temperatures under C2 and C3 conditions. This fact can be ascribed to the lower catalytic activity toward H_2 exchange of Cu-Pd coating as compared with Pt. Conversely, the values obtained under C4 are practically the same, indicating a similar catalytic activity for O_2 exchange. On the other hand, Cu coated membrane presents the lowest permeation under the three configurations which can be attributed to the lower catalytic activity toward both H_2 and O_2 exchange. These results are in agreement with the reported lower activity that Cu presents as compared with Pd and Pt for oxygen reduction and hydrogen evolution reactions.[22, 39] On the other hand, the catalytic surface area plays an important role, in addition to the intrinsic catalytic activity of each metal. The catalytic surface area differs depending on the coating process and the metal, i.e., Cu particles are smaller than Pd ones, that form a smooth layer as can be observed in Figure 8 and Figure 9. The catalytic activity of these layers could be further improved by controlling the particle size grown.

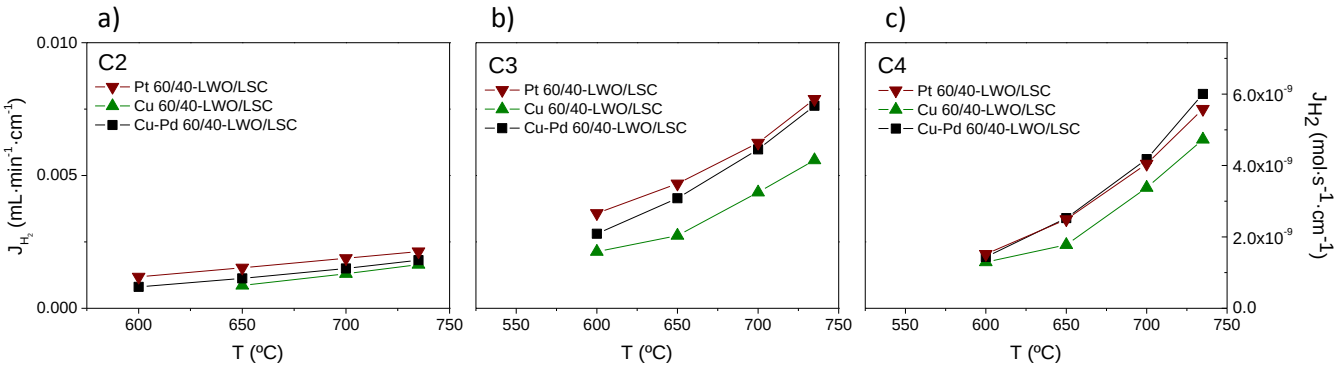

Figure 3: Comparison of the normalized H_2 flow (mL·min^{-1}·cm^{-1} and and mol·s^{-1}·cm^{-1}) obtained for 60/40-LWO/LSC with the sputtered metals and Pt as activation catalytic layers in hydration degree configurations (a) C2, (b) C3 and (c) C4. Experimental standard deviation ranges between 10^{-3} and 10^{-4}.

With the aim of evaluating the H_2 permeation and the stability of the Cu-Pd 60/40 LWO/LSC membrane, permeation test was performed by using 30% CH_4-50% H_2-20% He as feed gas under C4 conditions at 700 ºC. H_2 flows obtained as a function of time are plotted in Figure 4. H_2 flow steeply decreases when CH_4 is introduced in the feed stream and after a progressive decrease, it remains stable with a value of 0.12 mL·min^{-1}·cm^{-2}. When CH_4 is removed from the stream, the H_2 flow increases but the initial values are not fully reacovered, stabilizing in 0.134 mL·min^{-1}·cm^{-2}. The H_2 flows obtained and the stability of the measurement indicates that Cu-Pd 60/40 LWO/LSC membrane could be integrated in catalytic membrane reactors for steam methane reforming or methane dehydroaromatization reactions.

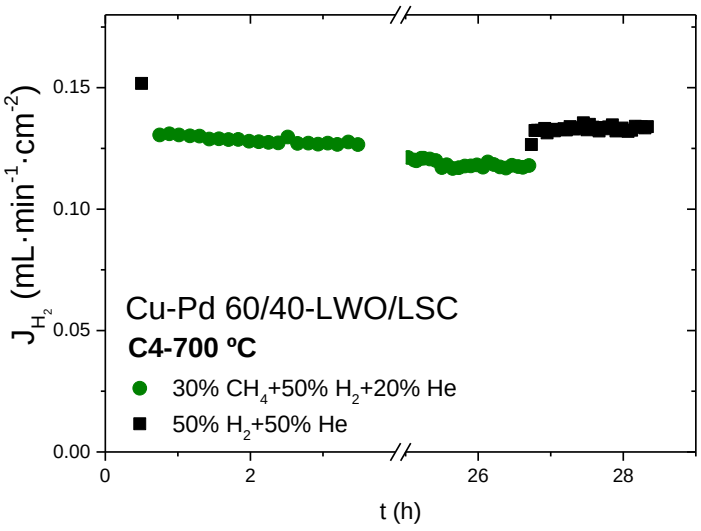

Figure 4: H_2 flow as a function of time for Cu-Pd sputtered membrane feeding 50% H_2 in He (black squares) and 30% CH_4-50% H_2 in He under C4 conditions at 700 ºC.

In order to check the higher catalytic activity of the Cu-Pd as compared with Cu layer, the electrochemical behavior of the two different metal sputtered layers was studied by EIS using symmetric cells made of BZCY72 electrolyte. First, compatibility of metal sputtered layers with BZCY72 was checked by XRD measurements and the morphology of the layers was studied by SEM and EDX analysis. Cu and Pd do not react with BZCY72 as can be observed in Figure 5a where only the diffraction peaks attributed to Cu and BZCY72 can be detected. Pd is not observed as it was explained for the LWO/LSC composite, but it can be detected by SEM analysis as it is shown in Figure 9 and Figure S1. Figure 5b and c show the SEM images of the Cu surface and the cross-section of the sample, respectively, where it can be observed that the thickness of the Cu layer was around 1.5 μm. Figure 5d-h presents the EDX mapping of the Cu sputtered layer on BZCY72 and it can be confirmed that there is no reaction between Cu layer and BZCY72 electrolyte, in agreement with previous reports[37].

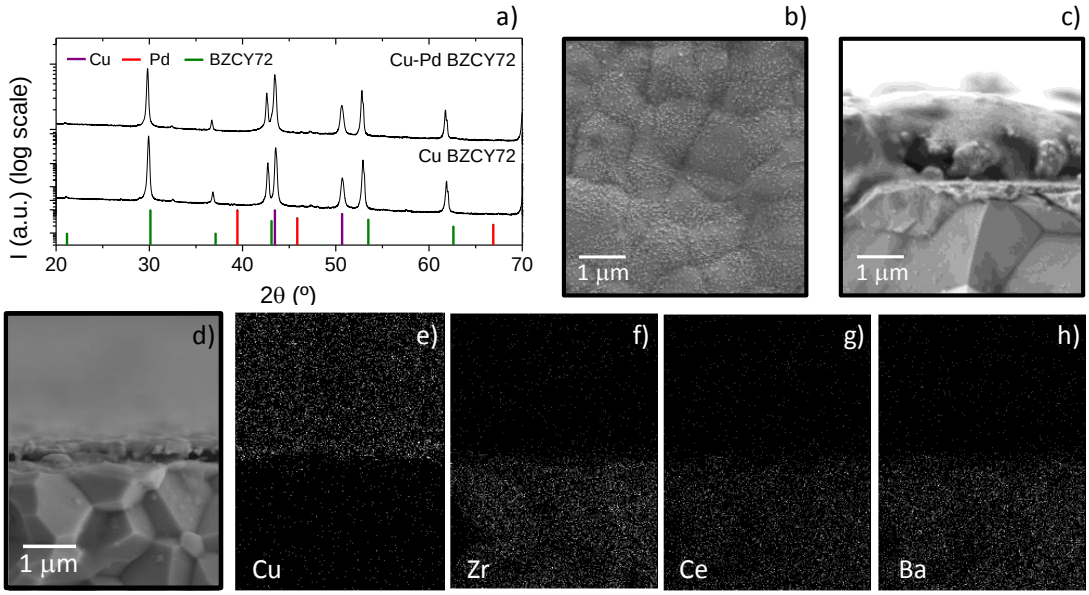

Figure 5: Characterization of BZCY72 electrolytes sputtered with Cu and Cu-Pd catalytic coatings: (a) XRD patterns; (b) SEM analysis of the top surface of the membrane; (c and d) fracture cross-sections; and (e-h) EDX mapping of the Cu sputtered layer on BZCY72 electrolyte.

The impedance spectra recorded at 700 ºC in wet 100% H_2 for the two metal sputtered catalytic layers are represented in Figure 6a and b (Nyquist and Bode plots, respectively).

The electrochemical performance is notably improved by the incorporation of Pd that decreases or eliminates low frequency (LF) contribution, and the performance slightly improves from 0.35 $\Omega \cdot cm^2$ for Cu to 0.29 $\Omega \cdot cm^2$ for Cu-Pd.

The polarization resistances (Rp) together with the fitted low (LF) and high frequency (HF) contributions in wet (2.5% H_2O) 100% H_2 and 5% H_2 in Ar are displayed as a function of temperature in Figure 6. LF contribution decreases one order of magnitude when Pd is sputtered whereas HF contribution is higher. The reduction of the LF process with the minor Pd addition can be directly associated with the improvement in surface kinetics since LF resistance are related to surface processes as catalytic reactions between chemisorbed species, adsorption/desorption reactions from/to the gas phase and surface diffusion of intermediate species.[40-44]

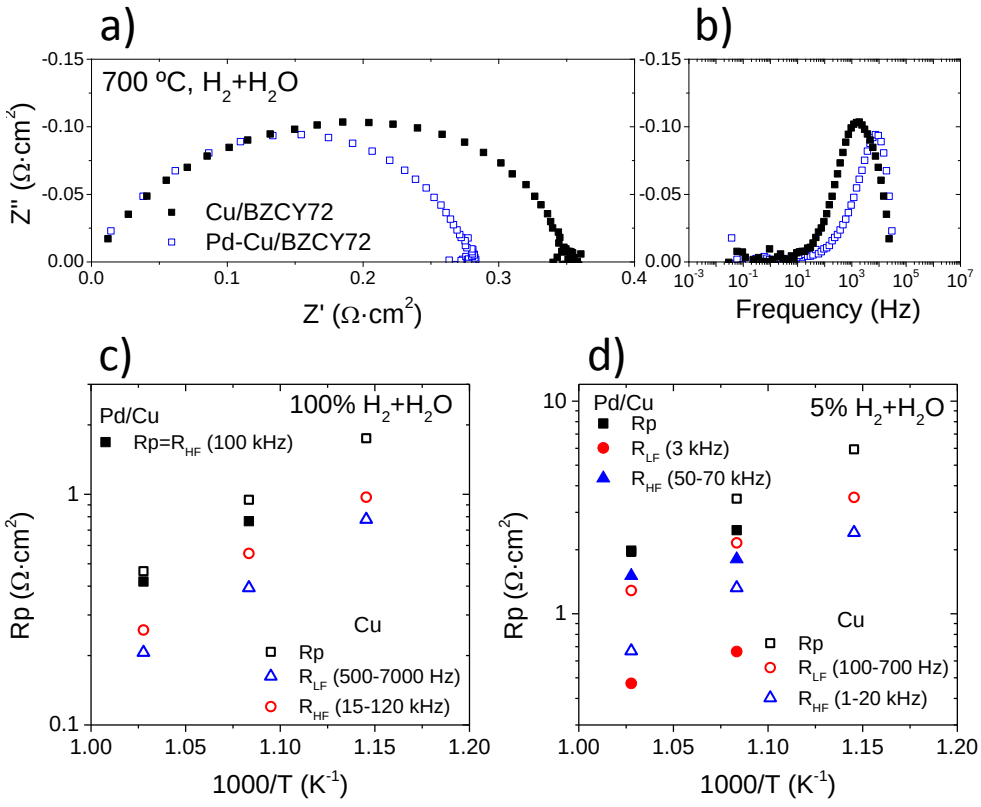

Figure 6: Nyquist (a) and Bode (b) plots of impedance spectra recorded in wet (2.5 % vol. H_2O) H_2 at 700 ºC for Cu/BCZY and Cu-Pd/BCZY. Modeled LF and HF resistances as a function of the temperature under wet 100% H_2 (c) and 5%H_2 in Ar (d).

Integrity of the samples was checked by XRD after the H_2 permeation measurements (including the measurements by feeding CH_4). No impurities or secondary phases are detected after the permeation measurements as can be observed in the XRD patterns

plotted in Figure 7. However, in the EIS experiments, continuous degradation of the Cu layer performance was observed when the sample was oxidized and then reduced again. On the contrary, if the sample is always in reducing conditions, the performance remains stable (wet and dry conditions).

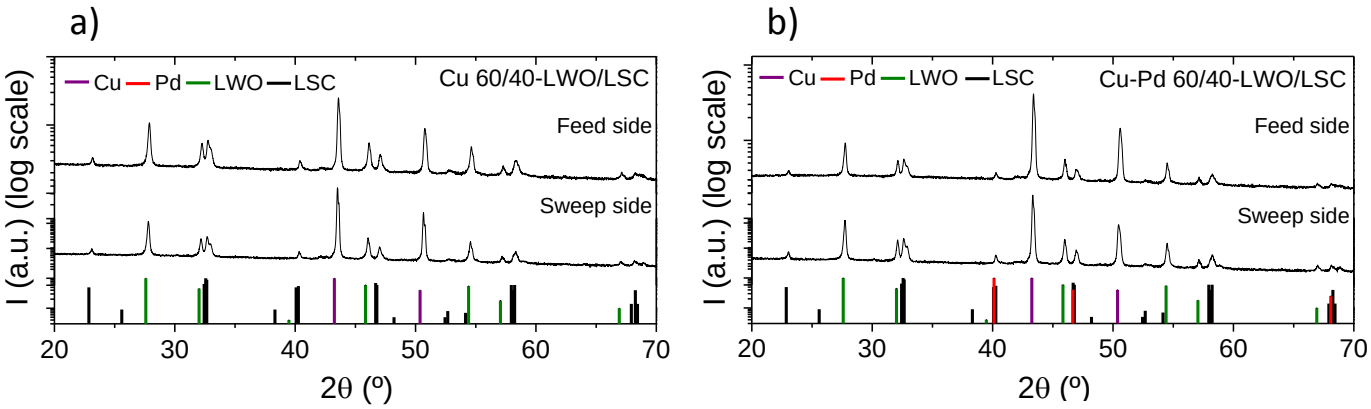

Figure 7: XRD patterns of 60%-LWO/LSC sputtered with (a) Cu and (b) Cu-Pd after the H_2 permeation measurements.

SEM analysis was also performed after H_2 permeation measurements. Figure 8 shows different magnifications of the surface of both sweep (a and b) and feed (d and e) sides together with the fractured cross sections (c and f, for feed and sweep sides respectively). The images show a continuous and porous Cu film of around 200 nm thickness and the formation of agglomerates, up to 2 μm size, in the sweep side. However, as can be seen in the low magnification image of the feed side (Figure 8g) the Cu grains are interconnected. Despite some Cu particles can be observed in some depressed areas due to the rough surface of the membrane, no conglomeration of the Cu particles could be detected in an specific area, as the grain boundaries, as it was previously observed for Ag catalytic layers.[25] The Cu films exhibited very good attachments to the composite membrane and no delamination occurs during permeation testing. However, the thickness of the sputtered layer was significantly reduced during the permeation tests (lasting ≈10 days). The initial thickness of the sputtered layer was around 1.5 μm and this was verified by the sputtering of a Si substrate at the same time than the LWO/LSC membranes (see SEM image in Figure S2).

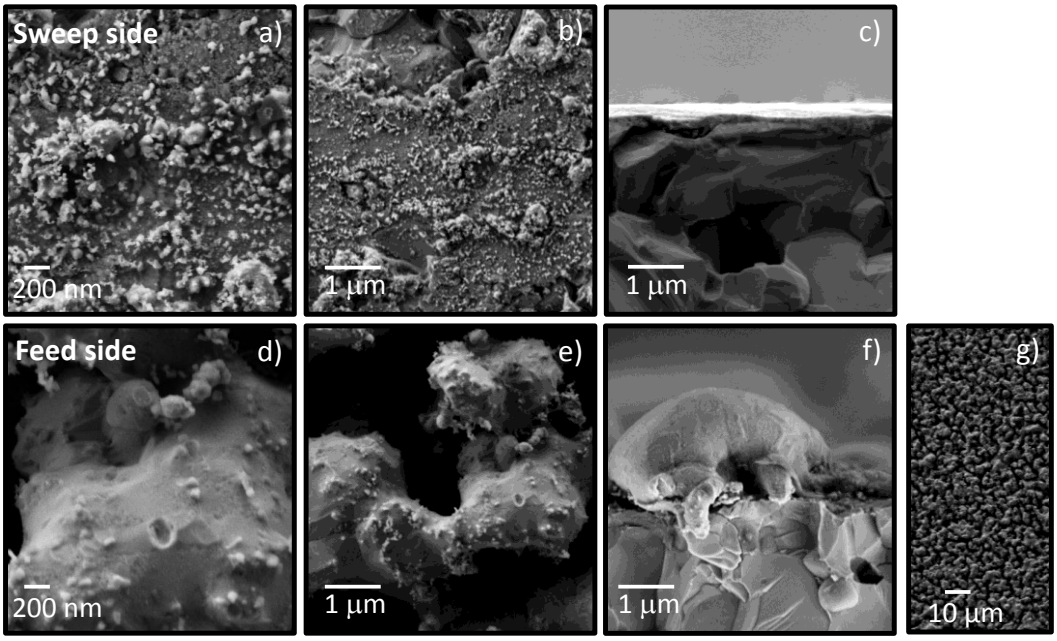

Figure 8: SEM analysis of the on top of the sweep (a and b) and feed (d, e and g) sides and corresponding fractured cross-sections (c and f, respectively) of the LWO/LSC sputtered with Cu after the H_2 permeation measurements.

Figure 9 shows the SEM analysis of the Cu-Pd catalytic layer with different magnifications of the surface morphology (a, b and c) and the cross section (d). From EDX analysis the Cu and Pd grains were identified (Figure 9b and Figure S1). Thus while the Cu grains present a very small grain size (of around 200 nm as can be observed in Figure 9a) the Pd grains are several microns long and spread along the surface of the Cu layer as can be seen in Figure 9c. Although the Pd grains do not cover completely the surface of the Cu layer they are connected, which allows a continuous effect of the Pd catalytic properties without blocking Cu ones. The cross section image (Figure 9d) shows a dense 60/40-LWO/LSC membrane and the Cu-Pd layer. This morphology, after the high temperature permeation measurements confirms the integrity of the catalytic layers under operation conditions.

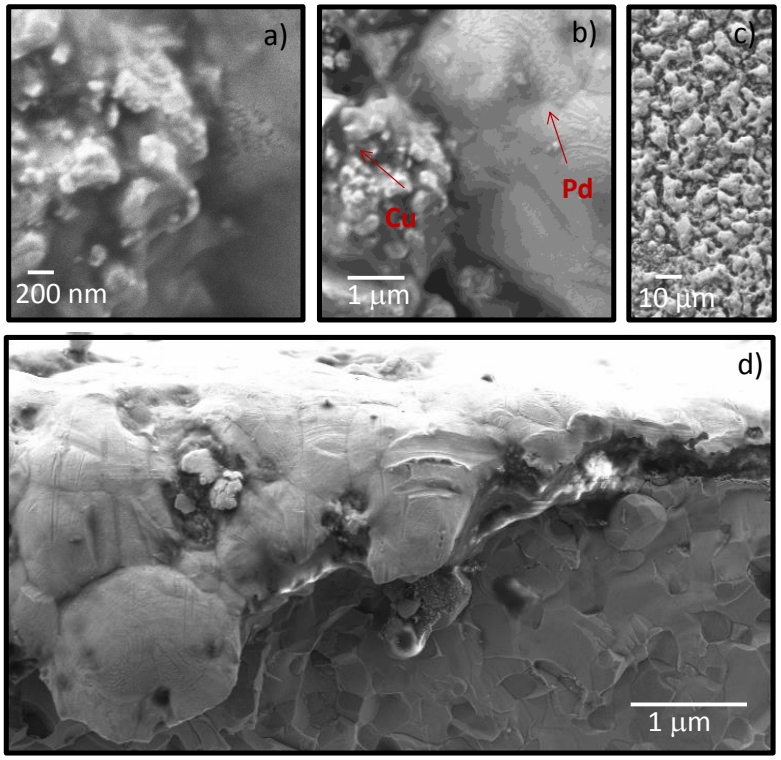

Figure 9: SEM analysis of the fractured cross-section of the 60/40-LWO/LSC membrane sputtered with Cu-Pd after the H_2 permeation measurements at different magnifications (a-d).

4. Conclusions

Metal sputtered catalytic layers were developed as potential H_2-activation layer for ceramic mixed protonic-electronic conducting membranes to be integrated in catalytic membrane reactors for steam methane reforming or methane dehydroaromatization reactions. Cu and Cu-Pd layers were deposited and the highest performance was obtained for the sample Cu-Pd 60%-LWO/LSC, reaching H_2 flows up to 0.22 $mL \cdot min^{-1} \cdot cm^{-2}$ under C3 conditions. This value is slightly lower than the corresponding when the composite membrane was screen-printed to produce a porous Pt thick-film. The higher surface catalytic activity of Cu-Pd coatings -compared to Cu coatings- was also observed in electrochemical test using a purely-protonic electrolyte (BZCY72) in symmetrical cell configuration. The electrochemical performance was improved by adding minor Pd loadings. Specifically, the resistance of LF processes was strongly reduced by Pd incorporation and this is directly associated to the surface kinetics enhancement. Finally, the integrity of the thin layers under permeation conditions was confirmed by XRD and SEM analysis.

Acknowledgements

Financial support by the Spanish Government (Grants ENE2014-57651 and SEV-2016-0683) and CoorsTek Membrane Sciences is kindly acknowledged. The support of the Servicio de Microscopía Electrónica of the Universitat Politècnica de València is also acknowledged.

Supporting Information

SEM and EDX analysis of Cu and Cu-Pd sputtered thin films.

TOC

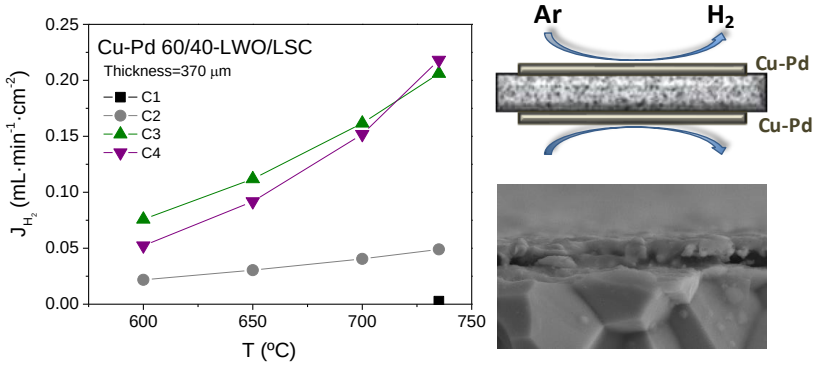
Cu-Pd 60/40-LWO/LSC
Thickness=370 μm
C1
C2
C3
C4
J_{H_2} (mL·min^{-1}·cm^{-2})
T (ºC)
0.25
0.20
0.15
0.10
0.05
0.00
600
650
700
750
Ar
H_2
Cu-Pd
Cu-Pd

References

1. Dittmeyer, R.; Höllein, V.; Daub, K., Membrane reactors for hydrogenation and dehydrogenation processes based on supported palladium. *Journal of Molecular Catalysis A: Chemical* **2001,** *173* (1–2), 135-184.

2. Jordal, K.; Bredesen, R.; Kvamsdal, H. M.; Bolland, O., Integration of H2-separating membrane technology in gas turbine processes for CO2 capture. *Energy* **2004,** *29* (9-10), 1269-1278.

3. Saracco, G.; Neomagus, H. W. J. P.; Versteeg, G. F.; Swaaij, W. P. M. v., High-temperature membrane reactors: potential and problems. *Chemical Engineering Science* **1999,** *54* (13–14), 1997-2017.

4. Liu, K.; Zhao, J.; Zhu, D.; Meng, F.; Kong, F.; Tang, Y., Oxidative coupling of methane in solid oxide fuel cell tubular membrane reactor with high ethylene yield. *Catalysis Communications* **2017,** *96*, 23-27.

5. Kinage, A. K.; Ohnishi, R.; Ichikawa, M., Marked enhancement of the methane dehydrocondensation toward benzene using effective Pd catalytic membrane reactor with Mo/ZSM-5. *Catalysis Letters* **2003,** *88* (3-4), 199-202.

6. Xue, J.; Chen, Y.; Wei, Y.; Feldhoff, A.; Wang, H.; Caro, J., Gas to Liquids: Natural Gas Conversion to Aromatic Fuels and Chemicals in a Hydrogen-Permeable Ceramic Hollow Fiber Membrane Reactor. *Acs Catalysis* **2016,** *6* (4), 2448-2451.

7. Li, L.; W. Borry, R.; Iglesia, E., Reaction-transport simulations of non-oxidative methane conversion with continuous hydrogen removal — homogeneous–heterogeneous reaction pathways. *Chemical Engineering Science* **2001,** *56* (5), 1869-1881.

8. Morejudo, S. H.; Zanon, R.; Escolastico, S.; Yuste-Tirados, I.; Malerod-Fjeld, H.; Vestre, P. K.; Coors, W. G.; Martinez, A.; Norby, T.; Serra, J. M.; Kjolseth, C., Direct conversion of methane to aromatics in a catalytic co-ionic membrane reactor. *Science* **2016,** *353* (6299), 563-566.

9. Cao, Z.; Jiang, H.; Luo, H.; Baumann, S.; Meulenberg, W. A.; Assmann, J.; Mleczko, L.; Liu, Y.; Caro, J., Natural Gas to Fuels and Chemicals: Improved Methane Aromatization in an Oxygen-Permeable Membrane Reactor. *Angewandte Chemie-International Edition* **2013,** *52* (51), 13794-13797.

10. Kniep, J.; Anderson, M.; Lin, Y. S., Autothermal Reforming of Methane in a Proton-Conducting Ceramic Membrane Reactor. *Industrial & Engineering Chemistry Research* **2011,** *50* (22), 12426-12432.

11. Kyriakou, V.; Garagounis, I.; Vourros, A.; Vasileiou, E.; Manerbino, A.; Coors, W. G.; Stoukides, M., Methane steam reforming at low temperatures in a

BaZr0.7Ce0.2Y0.1O2.9 proton conducting membrane reactor. *Applied Catalysis B-Environmental* **2016,** *186*, 1-9.

12. Gallucci, F.; Fernandez, E.; Corengia, P.; Annaland, M. v. S., Recent advances on membranes and membrane reactors for hydrogen production. *Chemical Engineering Science* **2013,** *92*, 40-66.

13. Escolastico, S.; Solis, C.; Kjolseth, C.; Serra, J. M., Outstanding hydrogen permeation through CO2-stable dual-phase ceramic membranes. *Energy & Environmental Science* **2014,** *7* (11), 3736-3746.

14. Escolástico, S.; Kjølseth, C.; Serra, J. M., Catalytic activation of ceramic H2 membranes for CMR processes. *Journal of Membrane Science* **2016,** *517*, 57-63.

15. Cheng, S.; Wang, Y.; Zhuang, L.; Xue, J.; Wei, Y.; Feldhoff, A.; Caro, J.; Wang, H., A Dual-Phase Ceramic Membrane with Extremely High H-2 Permeation Flux Prepared by Autoseparation of a Ceramic Precursor. *Angewandte Chemie-International Edition* **2016,** *55* (36), 10895-10898.

16. Fang, S.; Wang, S.; Brinkman, K. S.; Su, Q.; Wang, H.; Chen, F., Relationship between fabrication method and chemical stability of Ni-BaZr0.8Y0.2O3-delta membrane. *Journal of Power Sources* **2015,** *278*, 614-622.

17. Ivanova, M. E.; Escolastico, S.; Balaguer, M.; Palisaitis, J.; Sohn, Y. J.; Meulenberg, W. A.; Guillon, O.; Mayer, J.; Serra, J. M., Hydrogen separation through tailored dual phase membranes with nominal composition BaCe0.8Eu0.2O3-delta:Ce0.8Y0.2O2-delta at intermediate temperatures. *Scientific Reports* **2016,** *6*.

18. Polfus, J. M.; Xing, W.; Fontaine, M.-L.; Denonville, C.; Henriksen, P. P.; Bredesen, R., Hydrogen separation membranes based on dense ceramic composites in the La27W5O55.5-LaCrO3 system. *Journal of Membrane Science* **2015,** *479*, 39-45.

19. Rebollo, E.; Mortalo, C.; Escolastico, S.; Boldrini, S.; Barison, S.; Serra, J. M.; Fabrizio, M., Exceptional hydrogen permeation of all-ceramic composite robust membranes based on BaCe0.65Zr0.20Y0.15O3-delta and Y- or Gd-doped ceria. *Energy & Environmental Science* **2015,** *8* (12), 3675-3686.

20. Polfus, J. M.; Xing, W.; Sunding, M. F.; Hanetho, S. M.; Dahl, P. I.; Larring, Y.; Fontaine, M.-L.; Bredesen, R., Doping strategies for increased oxygen permeability of CaTiO3 based membranes. *Journal of Membrane Science* **2015,** *482* (0), 137-143.

21. Escolastico, S.; Kjolseth, C.; Serra, J. M., Catalytic activation of ceramic H-2 membranes for CMR processes. *Journal of Membrane Science* **2016,** *517*, 57-63.

22. Rossmeisl, J.; Bessler, W. G., Trends in catalytic activity for SOFC anode materials. *Solid State Ionics* **2008,** *178* (31–32), 1694-1700.

23. Atkinson, A.; Barnett, S.; Gorte, R. J.; Irvine, J. T. S.; McEvoy, A. J.; Mogensen, M.; Singhal, S. C.; Vohs, J., Advanced anodes for high-temperature fuel cells. *Nature Materials* **2004,** *3* (1), 17-27.

24. Leo, A.; Motuzas, J.; Yacou, C.; Liu, S.; Serra, J. M.; Navarrete, L.; Drennan, J.; Julbe, A.; Diniz da Costa, J. C., Copper oxide - perovskite mixed matrix membranes delivering very high oxygen fluxes. *Journal of Membrane Science* **2017,** *526*, 323-333.

25. Leo, A.; Liu, S.; Diniz da Costa, J. C., The enhancement of oxygen flux on Ba0.5Sr0.5Co0.8Fe0.2O3−δ (BSCF) hollow fibers using silver surface modification. *Journal of Membrane Science* **2009,** *340* (1), 148-153.

26. Takeguchi, T.; Kikuchi, R.; Yano, T.; Eguchi, K.; Murata, K., Effect of precious metal addition to Ni-YSZ cermet on reforming of CH4 and electrochemical activity as SOFC anode. *Catalysis Today* **2003,** *84* (3–4), 217-222.

27. Ricote, S.; Patki, N.; Way, J. D., Influence of the Activation Catalyst on the Polarization Resistance of Electroless Cu Electrodes on BaCe0.1Zr0.8Y0.1O3-δ proton-Conducting Ceramics. *Meeting Abstracts* **2017,** *MA2017-01* (33), 1608.

28. Zheng, M.; Wang, S.; Li, M.; Xia, C., H-2 and CO oxidation process at the three-phase boundary of Cu-ceria cermet anode for solid oxide fuel cell. *Journal of Power Sources* **2017,** *345*, 165-175.

29. McIntosh, S.; Vohs, J. M.; Gorte, R. J., Impedance spectroscopy for the characterization of Cu-Ceria-YSZ anodes for SOFCs. *Journal of the Electrochemical Society* **2003,** *150* (10), A1305-A1312.

30. Gaudillere, C.; Navarrete, L.; Serra, J. M., Syngas production at intermediate temperature through H2O and CO2 electrolysis with a Cu-based solid oxide electrolyzer cell. *International Journal of Hydrogen Energy* **2014,** *39* (7), 3047-3054.

31. Ruiz-Trejo, E.; Irvine, J. T. S., Electrolysis of CO2 in a proton conducting membrane. *Solid State Ionics* **2013,** *252*, 157-164.

32. Karagiannakis, G.; Zisekas, S.; Stoukides, M., Hydrogenation of carbon dioxide on copper in a H+ conducting membrane-reactor. *Solid State Ionics* **2003,** *162*, 313-318.

33. Escolastico, S.; Schroeder, M.; Serra, J., Optimization of the Mixed Proton-Electronic Conducting Materials based on the (Nd5/6Ln1/6)5.5WO11.25-[small delta]. *Journal of Materials Chemistry A* **2014,** *26* (2), 982–992.

34. Escolastico, S.; Somacescu, S.; Serra, J. M., Tailoring mixed ionic-electronic conduction in H2 permeable membranes based on the system Nd5.5W1-xMoxO11.25-[small delta]. *Journal of Materials Chemistry A* **2015,** *3* (2), 719-731.

35. Escolástico, S.; Somacescu, S.; Serra, J. M., Solid State Transport and Hydrogen Permeation in the System Nd5.5W1−xRexO11.25−δ. *Chemistry of Materials* **2013,** *26* (2), 982-992.

36. Rebollo, E.; Mortalò, C.; Escolástico, S.; Boldrini, S.; Barison, S.; Serra, J. M.; Fabrizio, M., Exceptional hydrogen permeation of all-ceramic composite robust membranes based on BaCe0.65Zr0.20Y0.15O3-δ and Y- or Gd-doped ceria. *Energy and Environmental Science* **2015,** *8* (12), 3675-3686.

37. Patki, N. S.; Ricote, S.; Way, J. D., Fabrication of reducing atmosphere electrodes (fuel electrodes) by electroless plating of copper on BaZr<inf>0.9</inf><inf>−</inf><inf>x</inf>Ce<inf>x</inf>Y<inf>0.1</inf>O<inf>3 </inf><inf>−</inf><inf>Δ</inf> – A proton-conducting ceramic. *International Journal of Hydrogen Energy* **2017,** *42* (27), 16911-16919.

38. Escolástico, S.; Serra, J. M., Nd<inf>5.5</inf>W<inf>1-x</inf>U<inf>x</inf>O<inf>11.25-δ</inf> system: Electrochemical characterization and hydrogen permeation study. *Journal of Membrane Science* **2015,** *489*, 112-118.

39. Greeley, J.; Markovic, N. M., The road from animal electricity to green energy: combining experiment and theory in electrocatalysis. *Energy & Environmental Science* **2012,** *5* (11), 9246-9256.

40. Sauvet, A. L.; Fouletier, J., Electrochemical properties of a new type of anode material La1−xSrxCr1−yRuyO3−δ for SOFC under hydrogen and methane at intermediate temperatures. *Electrochimica Acta* **2001,** *47* (6), 987-995.

41. Solís, C.; Vert, V. B.; Balaguer, M.; Escolástico, S.; Roitsch, S.; Serra, J. M., Mixed proton-electron conducting chromite electrocatalysts as anode materials for LWO-based solid oxide fuel cells. *ChemSusChem* **2012,** *5* (11), 2155-2158.

42. Solís, C.; Vert, V. B.; Fabuel, M.; Serra, J. M., Electrochemical properties of composite cathodes for La 0.995Ca0.005NbO4-δ-based proton conducting fuel cells. *Journal of Power Sources* **2011,** *196* (22), 9220-9227.

43. Solis, C.; Navarrete, L.; Bozza, F.; Bonanos, N.; Serra, J. M., Catalytic Surface Promotion of Composite Cathodes in Protonic Ceramic Fuel Cells. *Chemelectrochem* **2015,** *2* (8), 1106-1110.

44. Samson, A.; Sogaard, M.; Knibbe, R.; Bonanos, N., High Performance Cathodes for Solid Oxide Fuel Cells Prepared by Infiltration of La0.6Sr0.4CoO3-delta into Gd-Doped Ceria. *Journal of the Electrochemical Society* **2011,** *158* (6), B650-B659.